ARTICLE

Spectroscopic evidences to understand the influence of marine environments on Built Heritage

Héctor Morillas,[a] Maite Maguregui[b] and Juan Manuel Madariaga[a]
[a]Department of Analytical Chemistry, Faculty of Science and Technology, University of the Basque Country UPV/EHU, PO Box 644, 48080 Bilbao, Basque Country, Spain. E-mail: hector.morillas@ehu.es
[b]Department of Analytical Chemistry, Faculty of Pharmacy, University of the Basque Country UPV/EHU, PO Box 450, 01080 Vitoria-Gasteiz, Basque Country, Spain

Introduction

Marine aerosols are chemically complex systems formed by inorganic salts and organic matter, together with airborne particulate matter from the surrounding environment. The primary particles transported in marine aerosols (PMA) can cause different chemical reactions in the atmosphere, promoting formation of so-called Secondary Marine Aerosol (SMA) particles.

These kinds of particles, together with the natural crustal or mineral particles and the metallic airborne particulate matter emitted by anthropogenic sources (road traffic, industry etc.), can be deposited on building materials from a specific construction following wet or dry deposition processes.[1–3]

The interactions of the natural and anthropogenic stressors present in marine atmospheres with building materials immersed within these kinds of atmospheres result in the formation of different types of pathologies. Examples of this are the alveolisations or loss of material, which are the consequence of salts (marine aerosol) deposition/redissolution cycles on the surface of façades,[4] or water infiltrations containing harmful ions,[5–7] which can penetrate the pores of a material by capillarity, forming in some cases efflorescence. In other cases, biological patinas can be formed on the buildings'

materials, acting sometimes as protective or as degradation layers for the material itself.[8] SO_x emissions can also promote decaying processes on limestones[9] and carbonated sandstones.[3] This acid gas can be deposited following a wet process causing the formation of new sulfates on the material. These compounds, more soluble than carbonates, can be washed out due to the rainwater effect promoting the loss of material. On the other side, dry attack results in the formation of the so-called "black crusts", a patina made up of gypsum ($CaSO_4 \cdot 2H_2O$) in which atmospheric particulate matter (crustal and metallic particles, organic compounds, soot etc.) is trapped.

In this work, the usefulness of a non-invasive analytical methodology based on the application of molecular (Raman spectroscopy) and elemental (X-ray Fluorescence, XRF) spectroscopic techniques (both single point and imaging analysis) was tested to understand the negative influence exerted by marine environments (with or without the influence of urban–industrial activities) on the conservation state of building materials close to the sea.

Instrumentation

The molecular analysis was performed using three different Raman spectrometers, all of them with an excitation

laser of 785 nm: (a) a portable Raman spectrometer (innoRam, B&W Tek Inc., USA), (b) a Raman microprobe (RA100, Renishaw, UK) and (c) a confocal Raman microscope (inVia, Renishaw, UK) equipped with a 20× and 50× objectives.

For the elemental analyses, the M4 Tornado benchtop instrument (Bruker Nano GmbH, Berlin, Germany) was used, with single point and imaging analysis options, operated under vacuum and equipped with a microfocus side window Rh tube (powered by a low-power HV generator working at a maximum voltage of 50 kV and at a maximum current of 700 µA) and implementing a mechanical collimator allowing one to acquire measurements under 1 mm lateral resolution.

Buildings object of studies

Two buildings located in marine environments were considered for this work. One, the Igueldo lighthouse (San Sebastian) with direct marine and diffuse influence from an urban–industrial area was studied. In this historical building, cementitious materials, bricks, limestones and gypsum plasters were analysed. The other study was of sandstones from La Galea Fortress (Getxo), a building with direct marine and direct influence of a nearby urban–industrial area.

Table 1. Summary of the characteristic Raman bands of some decay compounds identified in the building materials from the Igueldo Lighthouse and La Galea Fortress.

Decay compounds	Mineral name	Building materials	ν (cm^{-1})
$CaSO_4 \cdot \frac{1}{2} H_2O$	Bassanite	Bricks, sandstone, limestones, mortars, cements & gypsum plasters	429 m, 487 m, 627 m, 668 m, 1015 vs, 1128 m
$CaSO_4$	Anhidrite type III	Bricks, sandstone, Llmestones, mortars, cements & gypsum Plasters	420 m, 490 m, 630 m, 673 m, 1025 vs, 1167 m.
$Na_3(SO_4)(NO_3) \cdot H_2O$	Darapskite	Gypsum plasters	472 vw, 619 w, 640 w, 707 w, 729 w, 993 s, 1059 vs, 1084 w, 1122 vw, 1354 w, 1416 w.
$Na_4Ca(SO_4)_3 \cdot H_2O$	Eugsterite	Gypsum plasters	1084 s, 1124 s
$K_3Na_7Mg_2(SO_4)_6(NO_3)_2 \cdot 6H_2O)$	Humberstonite	Gypsum plasters	184 vw, 217 m, 457 vw, 611 m, 632 s, 722 s, 1013 vs, 1048 vs, 1067 s.
$K_2Ca(SO_4) \cdot H_2O$	Syngenite	Gypsum plasters	441 s, 472 m, 492 w, 603 m, 621 m, 633 m, 642 m, 661 m, 981 vs, 1006 vs, 1082 m, 1119 m, 1139 w, 1165 m.
$K_2Ca_2Mg(SO_4)_4 \cdot 2H_2O$	Polyhalite	Gypsum plasters	236 m, 438 m, 465 s, 623 vw, 653 m, 989 s, 1016 vs, 1071 m, 1093 m, 1131 m, 1165 m.
$CaNa_2(SO_4)_2$	Glauberite	Gypsum plasters	453 w, 471 s, 485 m, 619 m, 624 m, 636 m, 644 s, 1001 vs, 1106 w, 1139 s, 1156 m, 1169 m
$(NH_4)_2SO_4$	Mascagnite	Sandstones, bricks	449 m, 614 w, 622 w, 974 vs, 1104 vw, 1417 vw.
$CaSO_4 \cdot 2H_2O$	Gypsum	Bricks, sandstone, limestones, mortars, cements & gypsum plasters	413 m, 492 m, 619 m, 673 m, 1008 vs, 1132 m.
K_2SO_4	Arcanite	Limestones and sandstones	455 m, 619 m, 988 vs, 1092 w, 1103 w, 1144 vw.
$Fe_2(SO_4)_3 \cdot 9H_2O$	(para)coquimbite	Mortars, limestones and sandstones	500 m, 600 w, 1025 vs, 1094 vw, 1176 vw, 1197 vw.
$MgSO_4 \cdot 4H_2O$	Starkeyite	Limestones and sandstones	147 w, 232 w, 312 w, 462 m, 613 m, 1001 vs, 1084 vw, 1115 vw, 1155 vw, 1603 vw.
$MgSO_4 \cdot 6H_2O$	Hexahydrite	Limestones and sandstones	249 w, 361 w, 442 w, 464 vw, 603 w, 982 vs, 1083 vw, 1148 vw.
$MgSO_4 \cdot 7H_2O$	Epsomite	Limestones and sandstones	362 vw, 445 w, 462 w, 609 w, 985 vs, 1082 vw, 1145 vw.
$BaSO_4$	Baryte	Limestones and sandstones	460 s, 618 m, 648 m, 987 vs, 990 vs, 1084 m, 1104 m, 1141 w, 1169 m.
$[Ca_6Al_2(OH)_{12}(SO_4)_3 \cdot 26H_2O]$	Ettringite	Cements	218 w, 361 vw, 448 m, 544 m, 648 m, 857 s, 890 m, 986 vs, 1061 m.
Na_2SO_4	Thenardite	Bricks, mortars, cements, limestones and sandstones	450 w, 465 w, 621 m, 632 m, 647 m, 992 vs, 1101 m, 1132 m, 1152 m.
$Na_2SO_4 \cdot 10H_2O$	Mirabilite	Bricks, mortars, cements, limestones and sandstones	446 w, 458 w, 616 m, 628 m, 989 vs, 1108 m, 1120 m, 1130 m.
KNO_3	Niter	Bricks mortars, limestones and sandstones	712 w, 1342 w, 1357 w, 1048 vs, 1777 vw.
$Ca(NO_3)_2 \cdot 4H_2O$	Nitrocalcite	Bricks, mortars, limestones and sandstones	719 w, 745 w, 1048 vs, 1352 w, 1437 m, 1640 vw.
$NaNO_3$	Nitratine	Bricks, mortars, limestones and sandstones	188 m, 414 vw, 518 vw, 533 vw, 722 s, 1067 vs, 1383 w, 1663 vw, 1775 vw.
$Ba(NO_3)_2$	Nitrobarite	Limestones and sandstones	200 w, 731 m, 1025 vw, 1046 vs, 1402 vw, 1631 vw,
$Mg(NO_3)_2$	Nitromagnesite	Cements, limestones and sandstones	729 s, 1059 vs, 1359 m, 1432 w.
NH_4NO_3	Nitrammite	Limestones and sandstones	714 s, 1040 vs, 1288 w, 1412 w, 1464 w, 1654 m.

vs, very strong; s, strong; m, medium; w, weak.

Analytical approach

First, an *in situ* screening of the aforementioned building materials was performed using a portable Raman spectrometer in order to extract preliminary results. After that, samples were extracted from selected areas and they were analysed in-depth in the laboratory using micro-Raman spectroscopy and energy-dispersive-XRF (ED-XRF).

Results and discussion

The different decay compounds detected by Raman spectroscopy in the building materials from Igueldo Lighthouse and La Galea Fortress are summarised in Table 1. These
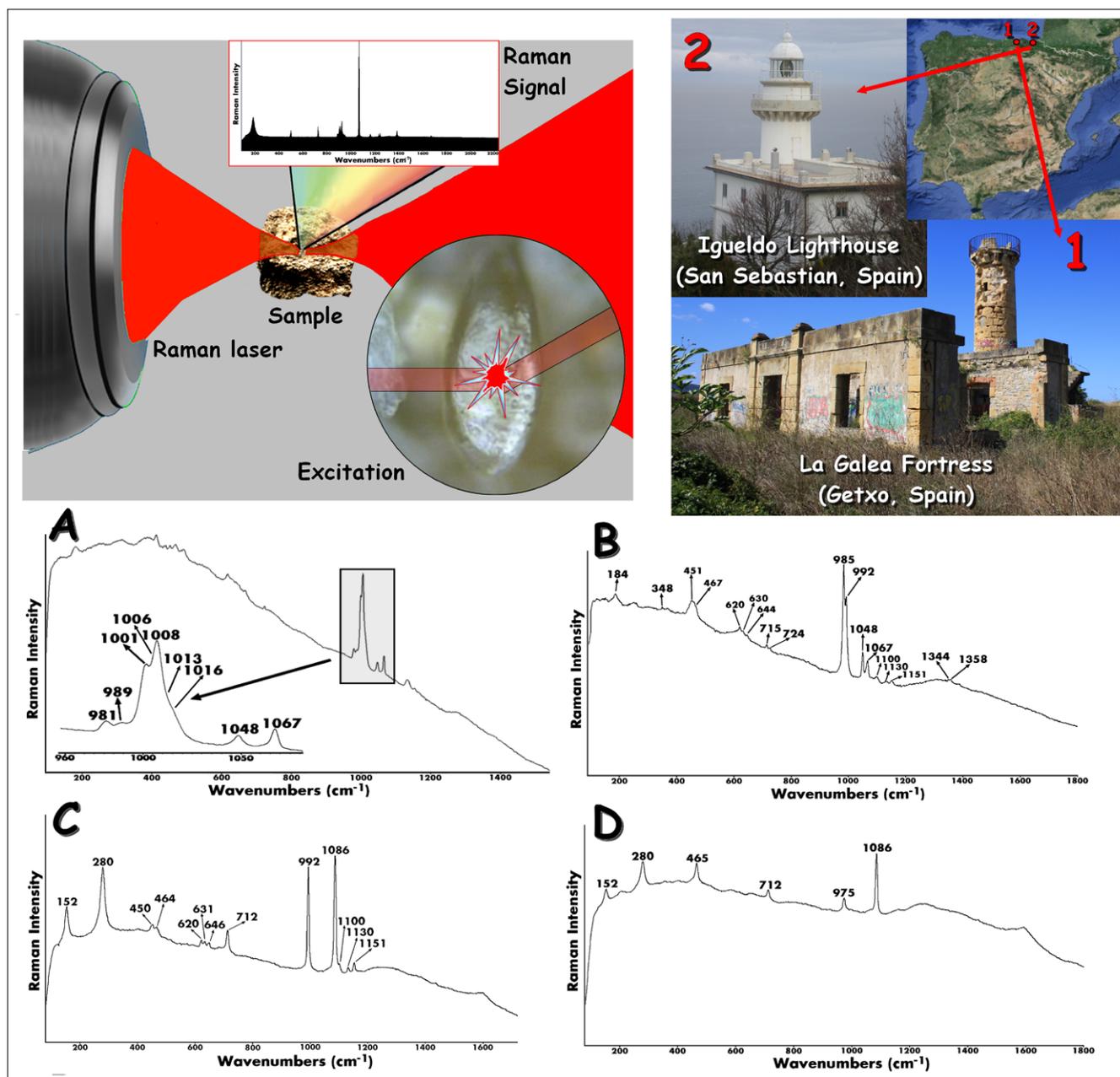
ARTICLE

Figure 1. Representation of a sample being analysed by Raman spectroscopy (top-left) and Igueldo Lighthouse and La Galea Fortress as building objects of study (top-right). (A) main Raman bands of gypsum, syngenite, glauberite, polyhalite and humberstonite on gypsum plasters from Igueldo Lighthouse; (B) main Raman bands of nitratine, niter, thenardite and epsomite on sandstone from La Galea Fortress; (C) main Raman bands of thenardite and calcite on sandstone from La Galea Fortress; and (D) main Raman bands of mascagnite and calcite on sandstone from La Galea Fortress.

compounds were formed by chemical reactions between the emissions and/or infiltration waters coming from both surrounding environments and the original compounds in the respective materials of the two buildings. In this sense, the formation of detected sulfates, nitrates and mixed sulfates–nitrates can only be explained by the reactivity between the wet deposition of atmospheric gaseous acids (CO_2, SO_2 and NO_x) on the carbonate compounds present in the original materials.

It is important to highlight that the combination of different molecular analysis techniques is necessary in order to confirm and complement the results obtained with only one analytical technique. In this sense, the combination of Raman spectroscopy and X-ray Diffraction is a good strategy to obtain complete molecular information. In some cases, if the analysed matrix is complex and lots of compounds are present, the Raman bands assignation is difficult. Even more so, if medium and weak bands related with each compound are not evident,

thereby making this task more difficult. As an example of this casuistry, in the Figure 1A different Raman bands obtained from gypsum plasters of the Igueldo Lighthouse are presented. The signals at 981 cm^{-1} and 1006 cm^{-1} (shoulder in 1000–1010 cm^{-1} region) correspond to syngenite [K$_2$Ca(SO$_4$)$_2$·H$_2$O], the band at 1001 cm^{-1} belongs to glauberite [CaNa$_2$(SO$_4$)$_2$], the bands at 989 cm^{-1} and 1016 cm^{-1} (shoulder in 1010–1030 cm^{-1} region) correspond to those of polyhalite [K$_2$Ca$_2$Mg(SO$_4$)$_4$·2H$_2$O] and the 1008 cm^{-1} peak to the main band of gypsum (CaSO$_4$·2H$_2$O). Finally, the bands at 1013 cm^{-1} (shoulder in 1010–1030 cm^{-1} region), 1048 cm^{-1} and 1067 cm^{-1} are clearly related with the bands of humberstonite [K$_3$Na$_7$Mg$_2$(SO$_4$)$_6$(NO$_3$)$_2$·6H$_2$O]. Analysing the whole spectrum shown in Figure 1A, the secondary bands of these mineral phases can also be ascertained.[4] As has been described in the literature, marine aerosols carry airborne particulate matter from sulfates and nitrates. Nitrate particles can be formed following a reaction between marine aerosol sea salts and NO$_x$ gases (NO$_2$, N$_2$O$_5$, ClONO$_2$ etc.) emitted into the atmosphere (e.g. road traffic source etc.). HNO$_3$ formed after the inclusion of NO$_{2(g)}$ in rainwater or humidity is reported to be the most important cause of the nitrate particles formation. These particles can react with building materials giving rise to different types of nitrate salts. An example of this is the presence of KNO$_3$ and NaNO$_3$ identified by Raman spectroscopy in the sandstone from La Galea Fortress (see Figure 1B). The bands at 1067 cm^{-1} and 724 cm^{-1} belong to nitratine (NaNO$_3$), while niter (KNO$_3$) was identified thanks to the presence of its main band at 1048 cm^{-1} and its secondary bands at 712 cm^{-1}, 1344 cm^{-1} and 1358 cm^{-1}. In this spectrum (Figure 1B) thenardite (Na$_2$SO$_4$, main band at 992 cm^{-1} and secondary bands at 451 cm^{-1}, 467 cm^{-1}, 620 cm^{-1}, 630 cm^{-1}, 644 cm^{-1}, 1100 cm^{-1}, 1130 cm^{-1} and 1151 cm^{-1}) was also detected. Apart from this compound, a band at 985 cm^{-1} was also observed, belonging to the main band of epsomite (MgSO$_4$·7H$_2$O). Marine aerosol can carry magnesium sulfates

with different hydration degrees. These sulfates can be deposited on the surface of the building materials as airborne particulate matter.[2,10,11]

In other cases (see Figure 1C), thenardite (Na$_2$SO$_4$) can be observed together with the presence of calcite (CaCO$_3$, main band at 1086 cm^{-1}, together with secondary bands at 712 cm^{-1} and 280 cm^{-1}). In Figure 1D, mascagnite [(NH$_4$)$_2$SO$_4$, the main Raman band at 975 cm^{-1}] was identified. Apart from this sulfate, peaks at 152 cm^{-1}, 280 cm^{-1}, 712 cm^{-1} and 1086 cm^{-1} belonging to calcite (CaCO$_3$) and 465 cm^{-1} belonging to quartz (SiO$_2$) were also detected. Mascagnite could be present in the material as airborne particulate matter present in the material following a dry deposition. The deposited ammonium sulfate can penetrate, dissolve and migrate to suffer a recrystallisation process in the inner parts of the material (sandstone) promoting loss of material during time.

In order to extract more information about the decaying compounds and the original composition of the materials, additional elemental analyses based on XRF were carried out. In the Figure 2, an exhaustive XRF analysis on the sandstone from La Galea Fortress is presented. In this case single point and imaging analyses were performed. As can be seen in the accumulated spectrum (see Figure 2 top-centre) of the imaging analysis (21.4 mm height × 25.9 mm width, 13,803 pixels) the presence of Al, Si, S, Cl, K, Ca, Ti, V, Mn, Fe, Co, Ni, Cu, Zn, Ga, Pb, As, Br, Rb, Sr, Y, Zr, Sn and Ba was detected. According to the semi-quantitative values determined by the software, Si, Al, Cl, K and Fe are present as major elements; S, Ca, Ti and Cu as minor elements; and the rest as trace elements. This observation confirms that this kind of sandstone has a considerable proportion of calcite. It is important to highlight that sometimes the bremsstrahlung continuum in the spectrum using a Rh tube can contribute to decrease the limit of detection for elements appearing at energies between 7 keV and 18 keV. To increase the limit of detection, lower electron acceleration voltages or filters can be used. An example regarding the

use of filters can be observed in Figure 2 top-right. In this case, due to the use of a 630 µm aluminium filter, the K-lines of Zn and As, elements present in trace levels in the sandstone can be observed more clearly when compared with the measurements without the filter.

Apart from single point analysis, XRF imaging helps us to observe different chemical tendencies along the sandstone. As can be observed in the Al–Si–K map (see Figure 2), pink areas representing the coincident Al–Si distribution are observable. Moreover, in some areas Si is also related with K (light blue areas) suggesting that some of the aluminosilicates in the sandstone could be present as potassium aluminosilicates. In this elemental map, dark blue areas are also highly distributed, representing the α-quartz presence, which is a major component in the sandstone. According to the Cl and Br maps (see Figure 2), these two elements are almost homogeneously distributed on the sandstone, confirming the deposition of these salts coming from the marine aerosol. In the Ca–Sr distribution map (see Figure 2) green areas are observable, representing the combined presence of Ca (yellow) and Sr (light blue). Calcium carbonate could contain Sr in its structure, thus it is not surprising to find a correlation between the distributions of both elements. This observation confirms the presence of calcite in this kind of stone, previously detected by Raman spectroscopy. However, in the same Ca–Sr distribution map, certain hot spots of Ca (yellow) and Sr (light blue) are observable. It is well-known that Sr is highly emitted by marine aerosol, thus Sr hot spots can be related with depositions of this element emitted by the marine aerosol.

In addition to chloride salts, marine aerosol also carries sulfate salts [e.g. arcanite or K$_2$SO$_4$)[2]]. Looking at the S–K map (see Figure 2), the distribution of both elements is coincident in certain areas (orange coloured regions), suggesting a possible deposition of arcanite or a possible chemical transformation of calcite present in the sandstone due to the SO$_2$ coming from the atmosphere. Finally, in the Ca–S distribution map background, pink areas can
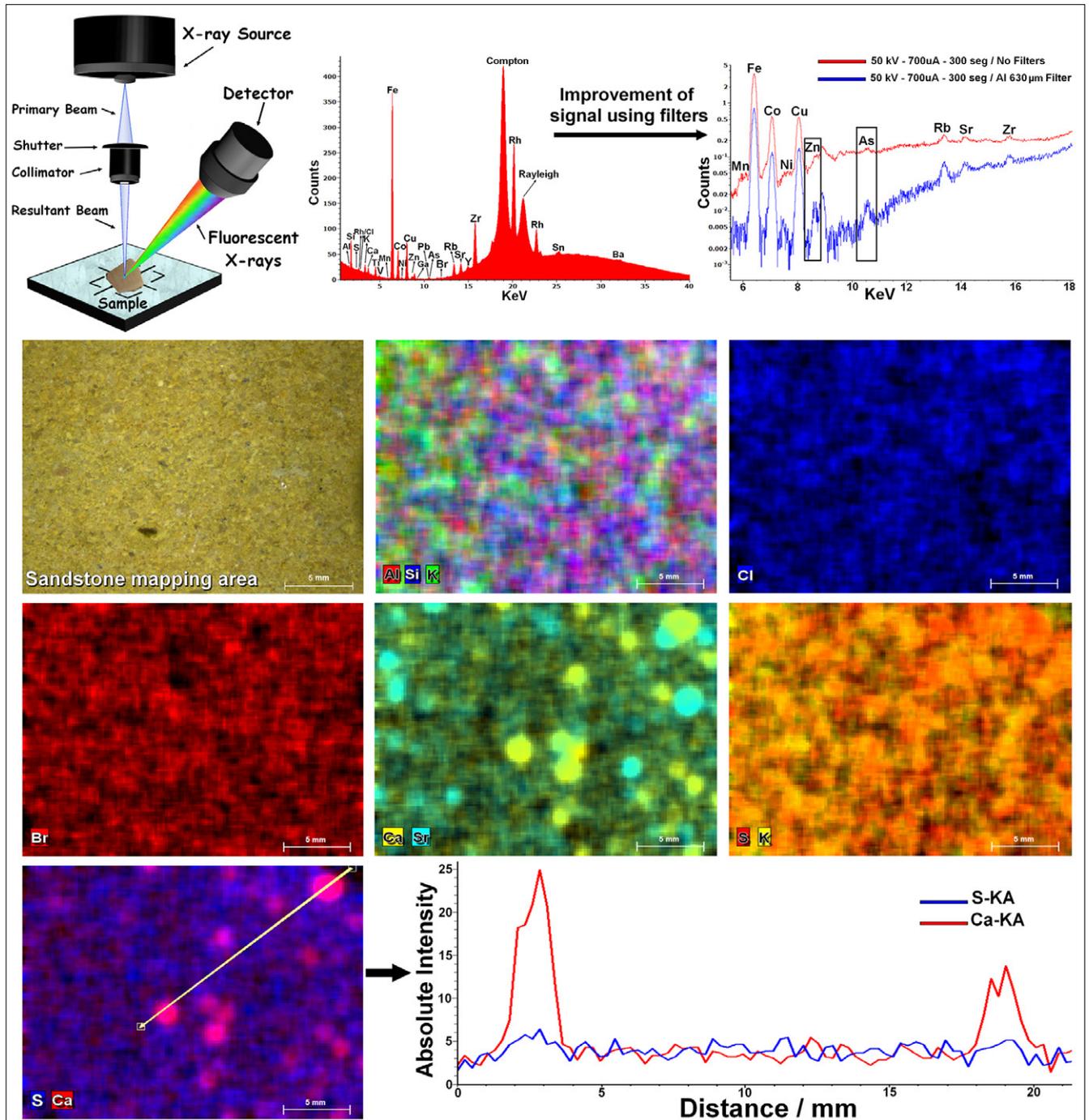
ARTICLE

Figure 2. Energy dispersive XRF spectrometer set up illustrating the measurement of a sandstone fragment from La Galea Fortress (top-left), the obtained XRF accumulated spectrum from the XRF imaging analysis (top-centre), spectral results obtained from the XRF single point analysis without (red) and with (blue) a 630 µm Al filter (top-right), Al–Si–K, Cl, Br, Ca–Sr, S–K, S–Ca distribution maps obtained from the XRF imaging analysis (see also the visible image of the mapped sandstone area) of the sandstone and a line scan (bottom-right) showing the variations of the Ca and S K-lines absolute XRF intensity (counts) in the line drawn in the S–Ca distribution map.

be observed. This coincidence in the distribution could point to a transformation of the calcite present in the sandstone into calcium sulfate due to the SO_2 coming from the atmosphere. On the contrary, the pink hotspots could suggest possible calcium sulfate depositions. Calcite particles can be emitted to the atmosphere due to the erosion of rocks. This carbonate compound can react in the atmosphere with the hydrated SO_2 acid gas (H_2SO_4) to give rise to calcium sulfate. This sulfate can suffer a subsequent deposition in the building materials following a dry deposition process. The higher signal input (absolute intensity in counts) of Ca and S in the hot spots can be observed in the line scan performed (see Figure 2 bottom-right).

Concluding remarks

In this study, it was possible to characterise different deterioration processes caused mainly by the influence of marine aerosols (wet and dry depositions), infiltration waters, salts migrations, atmospheric acid gases impact (wet and dry depositions) etc., due to the combined use of Raman spectroscopy and ED-XRF. The high amount of sulfates and nitrates present in these atmospheres coming from the marine aerosol itself or from acid gases (SO_2 and NO_x) emitted by urban–industrial sources can modify the original composition of these materials.

These results highlight the importance of the use of such analytical tools to detect the decay compounds and the original composition of the different materials from historical buildings close to the sea, which is fundamental in order to be able to explain the reactions that take place on them. This methodology can assist in the design of recovery actions and in the development of preventive conservation strategies for historical buildings.

Acknowledgements

References

1. H. Morillas, I. Marcaida, M. Maguregui, J.A. Carrero and J.M. Madariaga, "The influence of rainwater composition on the conservation state of cementitious building materials", *Sci. Total Environ.* **542,** 716–727 (2016). doi: http://dx.doi.org/10.1016/j.scitotenv.2015.10.041

2. H. Morillas, M. Maguregui, C. García-Florentino, I. Marcaida and J.M. Madariaga, "Study of particulate matter from Primary/Secondary Marine Aerosol and anthropogenic sources collected by a self-made passive sampler for the evaluation of the dry deposition impact on Built Heritage", *Sci. Total Environ.* **550,** 285–296 (2016). doi: http://dx.doi.org/10.1016/j.scitotenv.2016.01.080

3. H. Morillas, M. Maguregui, C. García-Florentino, J.A. Carrero, I. Salcedo and J.M. Madariaga, "The cauliflower-like black crusts on sandstones: A natural passive sampler to evaluate the surrounding environmental pollution", *Environ. Res.* **147,** 218–232 (2016). doi: http://dx.doi.org/10.1016/j.envres.2016.02.015

4. H. Morillas, M. Maguregui, C. Paris, L. Bellot-Gurlet, P. Colomban and J.M. Madariaga, "The role of marine aerosol in the formation of (double) sulfate/nitrate salts in plasters", *Microchem. J.* **123,** 148–157 (2015). doi: http://dx.doi.org/10.1016/j.microc.2015.06.004

5. H. Morillas, M. Maguregui, O. Gómez-Laserna, J. Trebolazabala and J.M. Madariaga, "Characterisation and diagnosis of the conservation state of cementitious materials exposed to the open air in XIX century lighthouses located on the coast of the Basque Country: The case of Igueldo lighthouse, San Sebastian, North of Spain", *J. Raman Spectrosc.* **43,** 1630–1636 (2012). doi: http://dx.doi.org/10.1002/jrs.4130

6. H. Morillas, M. Maguregui, O. Gómez-Laserna, J. Trebolazabala and J.M. Madariaga, "Could marine aerosol contribute to deteriorate building materials from interior areas of lighthouses? An answer from the analytical chemistry point of view", *J. Raman Spectrosc.* **44,** 1700–1710 (2013). doi: http://dx.doi.org/10.1002/jrs.4396

7. H. Morillas, M. Maguregui, J. Trebolazabala and J.M. Madariaga, "Nature and origin of white efflorescence on bricks, artificial stones, and joint mortars of modern houses evaluated by portable Raman spectroscopy and laboratory analyses", *Spectrochim. Acta A.* **136,** 1195–1203 (2015). doi: http://dx.doi.org/10.1016/j.saa.2014.10.006

8. H. Morillas, M. Maguregui, I. Marcaida, J. Trebolazabala, I. Salcedo and J.M. Madariaga, "Characterization of the main colonizer and biogenic pigments present in the red biofilm from La Galea Fortress sandstone by means of microscopic observations and Raman imaging", *Microchem. J.* **121,** 48–55 (2015). doi: http://dx.doi.org/10.1016/j.microc.2015.02.005

9. M. Hoyos, S. Sanchez-Moral, E. Sanz-Rubio and J.C. Canaveras, "Alteration causes and processes in the stone material from the pavement in Baelo Claudia archeological site, Cadiz/Spain", *Mater. Construcc.* **49,** 5–18 (1999). doi: http://dx.doi.org/10.3989/mc.1999.v49.i255.438

10. L.-Y. Zhao, Y.-H. Zhang, Z.-F. Wei, H. Cheng and X.-H. Li, "Magnesium sulfate aerosols studied by FTIR spectroscopy: hygroscopic properties, supersaturated structures, and implications for seawater aerosols", *J. Phys. Chem. A.* **110,** 951–958 (2006). doi: http://dx.doi.org/10.1021/jp055291i

11. S. Maskey, H. Geng, Y-C. Song, H. Hwang, Y-J. Yoon, K-H. Ahn and C.U. Ro, "Attenuated total reflection Fourier transform-infrared imaging techniques", *Environ. Sci. Technol.* **45,** 6275–6282 (2011). doi: http://dx.doi.org/10.1021/es200936m